Behaviour and Analysis of Horizontally Curved Steel Box-Girder Bridges

Scientific Research Publishing

Open Journal of Civil Engineering, 2022, 12, 390-414
https://www.scirp.org/journal/ojce
ISSN Online: 2164-3172
ISSN Print: 2164-3164

Behaviour and Analysis of Horizontally Curved Steel Box-Girder Bridges

Mattia Mairone[1*], Rebecca Asso[2], Davide Masera[3], Pietro Palumbo[1]

[1]Research and Development, Masera Engineering Group S.r.l, Corso Re Umberto 8, Torino, Italy
[2]Department of Structural, Geotechnical and Building Engineering DISEG, Politecnico di Torino, Corso Duca degli Abruzzi 24, Torino, Italy
[3]Masera Engineering Group S.r.l., Corso Re Umberto 8, Torino, Italy
Email: *mattia.mairone@masera-eg.com, rebecca.asso@polito.it, davide.masera@masera-eg.com, pietro.palumbo@masera-eg.com

How to cite this paper: Mairone, M., Asso, R., Masera, D. and Palumbo, P. (2022) Behaviour and Analysis of Horizontally Curved Steel Box-Girder Bridges. *Open Journal of Civil Engineering*, **12**, 390-414.
https://doi.org/10.4236/ojce.2022.123022

Received: August 19, 2022
Accepted: September 17, 2022
Published: September 20, 2022

Abstract

Various theories and analytical formulations were implemented and exploited in the 1980s and 1990s for the design of bridge beams or decks curved in the horizontal plane and subjected to out-of-plane loads. Nowadays, the Finite Element Method (FEM) is a valid tool for the analysis of structures with complex geometries and, therefore, the development of sophisticated analytical formulations is not needed anymore. However, they are still useful for the validation of FE models. This paper presents the case study of an existing viaduct built in North Italy, aiming to compare analytical approaches and numerical modelling. The bridge is characterized by an axis curved in two directions and a rectilinear segment. The global analysis of the viaduct is carried out with special attention to the attributes that cause torque action and bending moment. The theoretical developments focus on a deeper understanding of the torsional response under different constraint and loading conditions and aspire to raise awareness of the mutual interaction of flexural and torsional behaviour, that are always present in these complex curved systems. The examination of the case study is also obtained by comparing the response of isostatic and hyperstatic curvilinear steel box-girders.

Keywords

Analytical Calculation, Bridges, Horizontally Curved Beam, Structural Response, Torsion

1. Introduction

The use of horizontally curved steel girders in highway bridges has undergone remarkable developments over the past several decades [1]. When curved bridge

superstructures were first introduced, they were generally composed of a series of straight girder chords [2]. In the early years of modern bridge design, in fact, engineers were unwilling to use curved girders due to mathematical complexities [3] associated with their design.

Bridges with complex geometries or structures with curvilinear axis with variable radius [4] [5] are sometimes needed for the optimization of the road path [6] and minimization of the materials used. To deal with complex stress redistribution and torque [7], the superstructure of curvilinear viaducts can be characterized by decks with particular cross-sectional geometries, such as:

- Box deck with a single-cell, in composite steel-concrete, prestressing steel or steel materials (**Figure 1(a)**).
- Box beams interconnected with a slab (**Figure 1(b)**).
- Multicellular box decks in steel, prestressed concrete or composite systems (**Figure 1(c)**).
- Decks with I-section-beams in reinforced or prestressed concrete.

The use of closed sections has proved to be a very efficient structural solution for bridges and flyovers [8] thanks to the high torsional stiffness that is provided and the ability to efficiently distribute the eccentric variable traffic-load [9] [10] among the cores of the box-girder, together with maintainability, economy and aesthetics.

However, curvilinear bridge decks always show torsional deformation under vertical loads [1], due to an eccentricity between applied loads and support reactions [11]. Consequently, an interaction between bending and torsion moments occurs along the spans [12], that can be more easily analyzed with finite element models than with analytical calculations. However, when an analytical calculation is performed, bridges with curvilinear layout are considered as horizontally curved beam (HCB) in the horizontal plane [2].

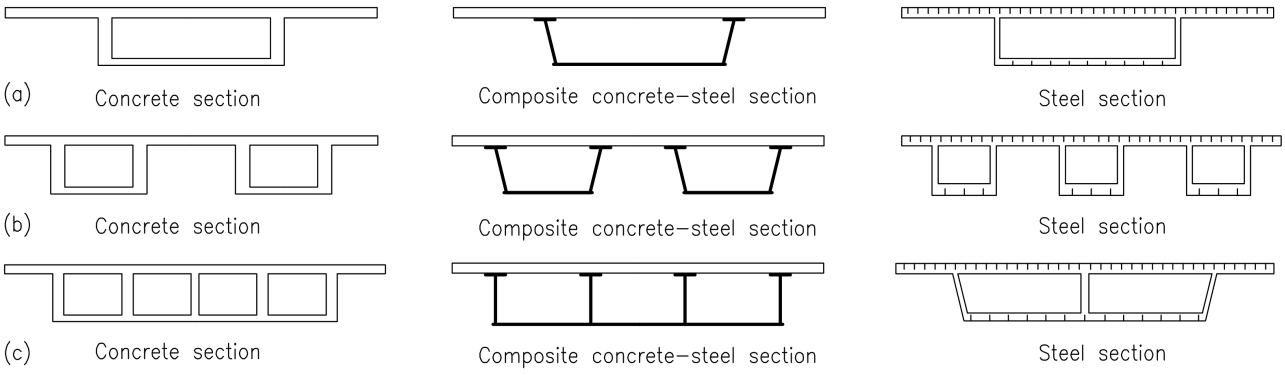

Figure 1. Types of box sections: (a) Single cell; (b) Interconnected single-cell; (c) Multicellular [7].

According to the type of cross-section, it is possible to describe the torsional behaviour [3] of bridge decks recalling two main categories:

- Open cross-section: often obtained either by two main beams (twin girder) or by several main beams (multi-girder). This system is essentially resisting

to non-uniform [13] (warping) torsional actions and provides limited torsional rigidity.

- Closed cross-section: it may comprise a box that is completely made of steel, a steel U shaped section or a twin girder section closed by lower plan bracing. Essentially, it resists in uniform (St-Venant) torsion and deforms very little. These systems are advantageous for bridges subjected to significant torsion such as, for example, curved bridges or bridges with substantial cantilevers to the slab.

In the present paper, a discussion about the different analytical and numerical approaches that can be used to design horizontally curved girders is proposed, with particular regard to the case study of a steel-box girder bridge. First, the analytical approach, originally used by the designers is recalled, which turns out to be strongly simplified and conservative with respect to the computations of the torque action. Then, an improved analytical evaluation of the torque action is proposed, which is based on a more realistic representation of the boundary conditions. Finally, finite elements method calculations are presented, having different level of details on the geometrical description of the bridge. The main aim is to highlight the advantages and disadvantages of the different approaches available for the design of such complex structures, namely analytical formulations and numerical models. The case study has been selected in order to deal with a simple bridge, with only three spans, but having the possibility to analyze different load and boundary conditions, which play a significant role in the interplay between bending and torque actions in these kinds of structures.

2. Case Study: The Viaduct

The case study concerns an existing viaduct in North Italy, which was designed at the end of the 1980s [14]. It consists of two independent carriageways (see **Figure 2**), both with three spans, supported by four reinforced concrete piers 35 m high. The Orthotropic Steel Deck, OSD made of S355 steel [15], is a box-girder with a height variable (see **Figure 3** and **Figure 4**) between 3 m at the two transversal joints and 5 m [16] in the central span. The North carriageway is 307.00 m long (93.50 m + 120.00 m + 93.50 m) while the South carriageway is 279.50 m (76.25 m + 120.00 m + 83.25 m).

The planimetric layout is characterized by a counterclockwise clothoid followed by a straight portion and then a clockwise clothoid (see **Figure 5**). The maximum radius of curvature is 1200 m (see **Table 1**). Multidirectional supports [17] consisting in PTFE bearings that allow displacements in transversal and longitudinal directions were placed in all piers (P9 to P12) except in pier P10 of both carriageways, where fixed supports were placed.

The permanent structural and non-structural loads [18], such as pavement and barriers, which were applied in the original structural design, are reported in **Table 2**.

Figure 2. View of the intrados of the central span.

Table 1. Geometric characteristics of the viaduct's spans.

GEOMETRIC CHARACTERISTICS OF THE DECK					
Span ID		**C1 (P9 - P10)**	**C2 (P10 - P11)**	**C3 (P11 - P12)**	
Radius of curvature	R	1200.00	1200.00	1200.00	[m]
Span length	L	76.33	120.00	83.25	[m]
Half-opening angle	ϕ_0	0.06361	0.10000	0.069375	[rad]

Table 2. Analysis of permanent loads used in original calculations design.

PERMANENT LOADS		
Self-weight	56.48	[kN/m]
Safety barriers	2 × 7.32 (eccentricity 6.12 m)	[kN/m]
Pavement layer	16.89	[kN/m]

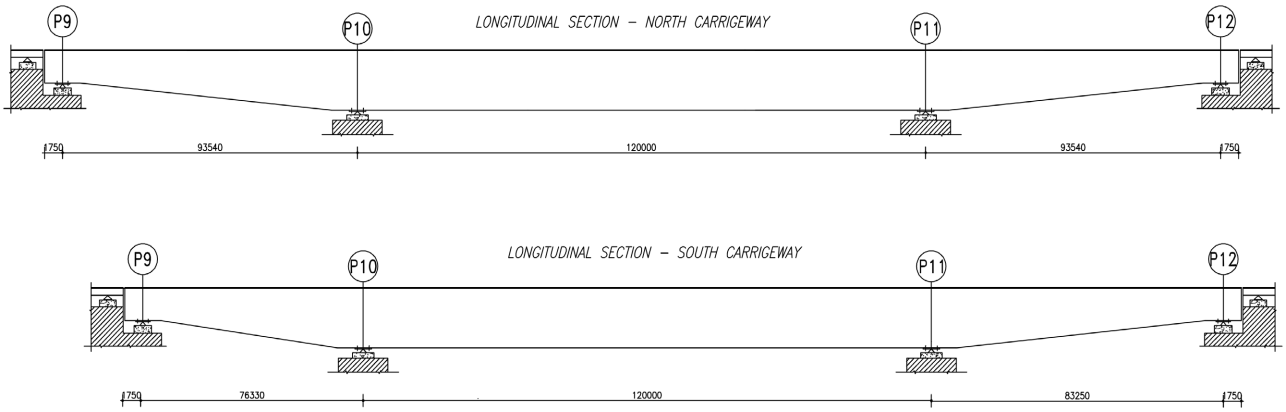

Figure 3. Longitudinal view of the two carriageways (dimensions in mm).

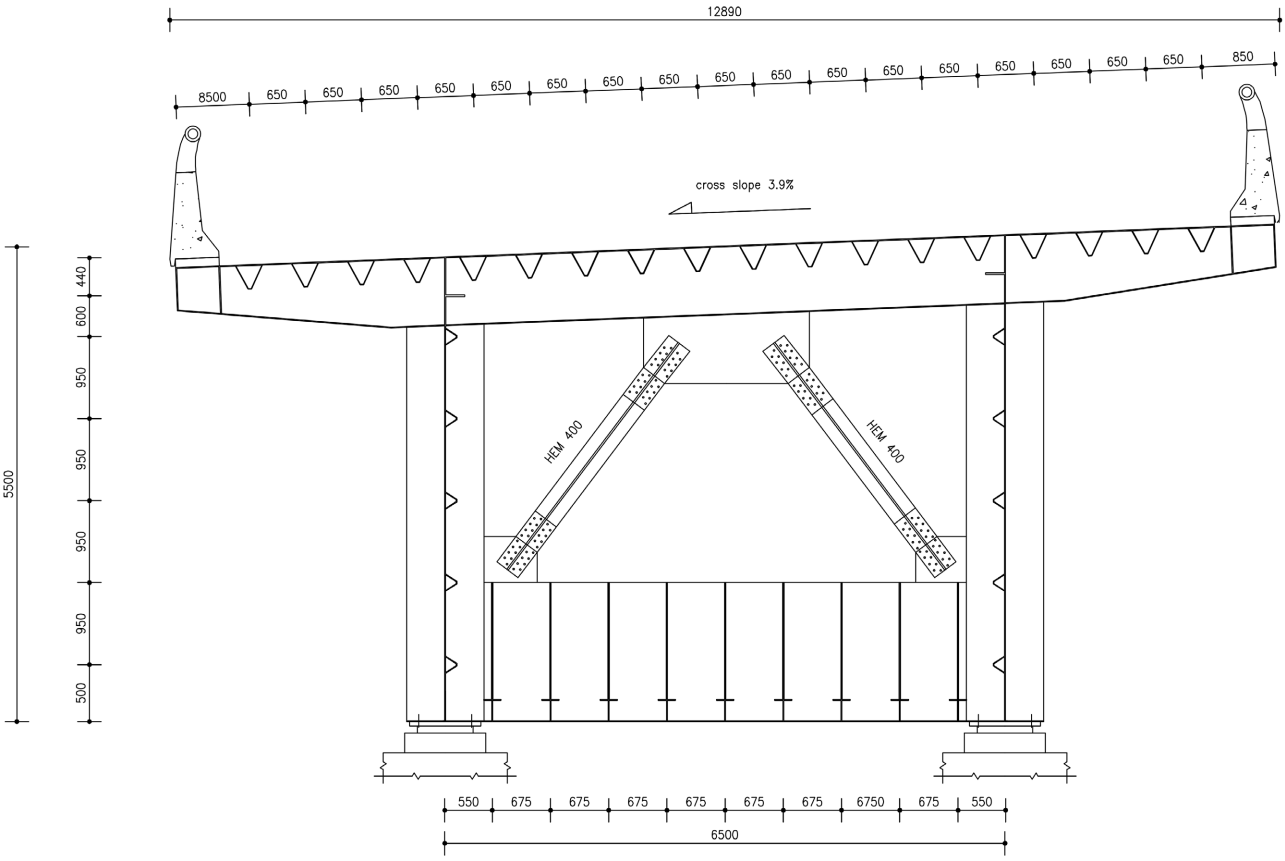

Figure 4. Transversal section of the deck in axis with piers P10 and P11.

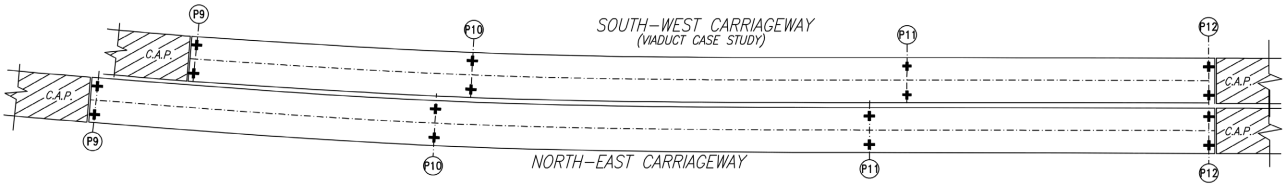

Figure 5. Plan view of the two carriageways.

3. Analytical Methodologies

The theoretical approach proposed in this paper aims to study simplified static schemes, *i.e.* each span is analyzed independently to the others by imposing appropriate boundary conditions and applying the uniformly distributed permanent structural and non-structural loads [19].

Moreover, different constraints are taken into account in order to validate the results of the complete FE model. The nomenclature and the general sign conventions are shown in Figure 6: for the specific situations the conditions of constraint at the piers P_i and P_j, are provided in Table 3. Given the particular configuration of the support devices of the viaduct object of study the torsional rotation at the pier axis is always constrained.

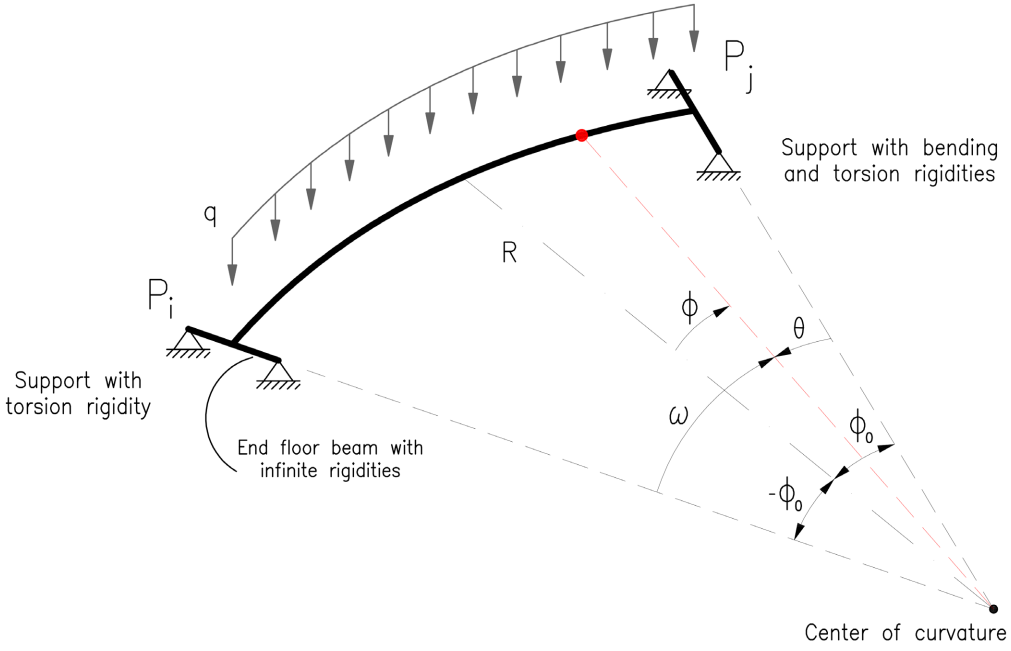

Figure 6. Generic structural model for a single span HCB.

Table 3. Comparison of constraints of the central span C2 (6 times statically indeterminate) and lateral spans C1 and C3 (3 times statically indeterminate).

BRIDGE SPAN	IN-PLANE DISPLACEMENT		BENDING ROTATION		TWISTING ROTATION	
	Node-i	Node-j	Node-i	Node-j	Node-i	Node-j
P9 - P10	Roller	Clamped-end	Free	Restrained	Restrained	
P10 - P11	Clamped-end		Restrained			
P11 - P12		Roller		Free		

The results of the HCB theory are used to validate the results of the global FE models (see Figure 7), under the action of the self-weight and the non-structural permanent loads.

Table 4. Geometric characteristics of the mean section of the three spans of the entire viaduct.

GEOMETRIC CHARACTERISTICS OF CROSS-SECTION					
SPAN ID		**C1 (P9 - P10)**	**C2 (P10 - P11)**	**C3 (P11 - P12)**	
Number of webs	n_w	2	2	2	[−]
Left cantilever	a	2.73	2.725	2.73	[m]
Right cantilever	b	6.50	6.000	6.50	[m]
Height of the box-girder	h	4.00	5.500	4.14	[m]
Upper flange thickness	t_s	0.034	0.300	0.034	[m]
Lower flange thickness	t_i	0.017	0.300	0.017	[m]
Webs thickness	t_w	0.017	0.300	0.017	[m]
Cross-section area	A	0.6528	8.535	0.6576	[m^2]
Lower static moment	$S_{X,\mathrm{INF}}$	1.8972	27.968	1.9735	[m^3]
Centroid abscissa	X_G	0.00	0.00	0.00	[m]
Centroid ordinate	$Y_{G,\mathrm{LOWER}}$	2.91	3.277	3.00	[m]
Ordinate of the centroid from the extrados	$y_{G,\mathrm{UPPER}}$	1.09	2.223	1.14	[m]
Moment of inertia with respect to X	I_X^G	1.7124	45.579	1.8454	[m^4]
Moment of inertia with respect to Y	I_Y^G	6.6606	72.642	6.7109	[m^4]
Internal shear area	$\Omega = 2A$	52.0000	66.000	53.8200	[m^2]
Geometric circuit	$H = \int_C \frac{\mathrm{ds}}{t(s)}$	1 044.12	76.667	1 060.59	[−]
Torsional stiffness factor	$J = \frac{4\Omega^2}{H}$	2.5898	56.832	2.7311	[m^4]

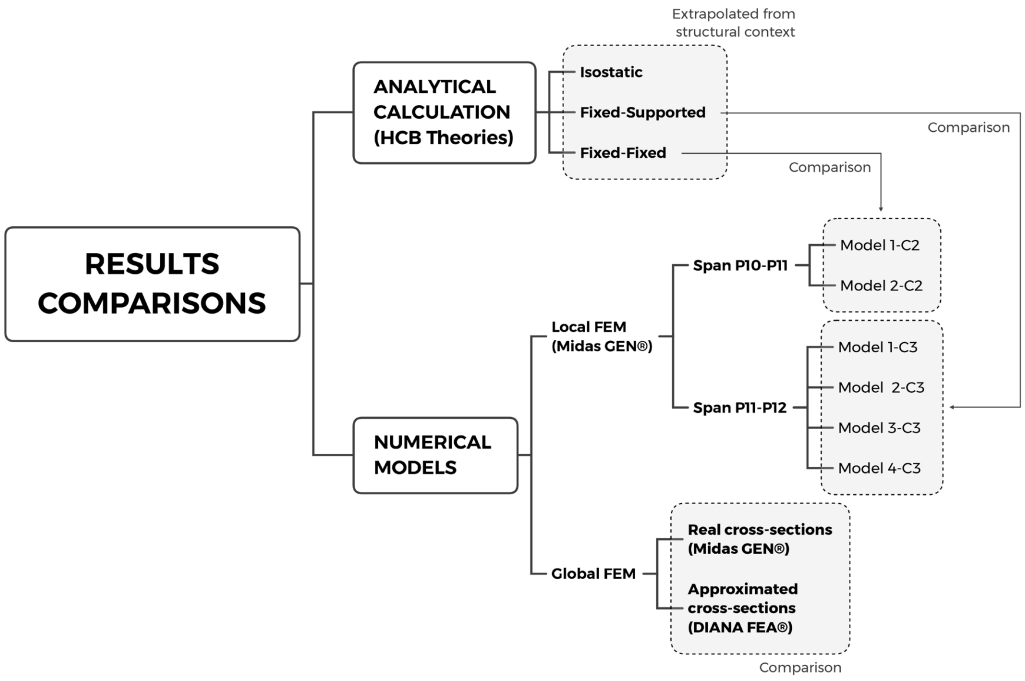

Figure 7. Comparisons between analytical calculation and FE models.

3.1. Original project

3.1.1. Isostatic HCB Theory for the Torque Moment

In the original project of the viaduct [20], the torque moment diagram in **Figure 8** was obtained using Equation (1), which provides a strong approximation of the real torsional structural behavior of the viaduct under study: the bending rotation at the beam ends is released, providing the maximum torsional stresses at the supports, according to ref. [21] and also considering that the bending moment is the first derivative of the torque ($\mathrm{d}T/\mathrm{d}\phi = M$):

$$T(\phi) = q \cdot R^2 \cdot \left[\frac{\cos(\phi)}{\operatorname{sen}(\phi_0)} - \phi \right] \tag{1}$$

whereas the shear diagram is given by Equation (2):

$$V(\phi) = q \cdot R \cdot \phi \tag{2}$$

where R is the radius of curvature; ϕ is the angle defined by a generic point with respect to the mid-span of the beam; q is the uniformly distributed load; $T(\phi)$ is torque moment and $V(\phi)$ is the shear force.

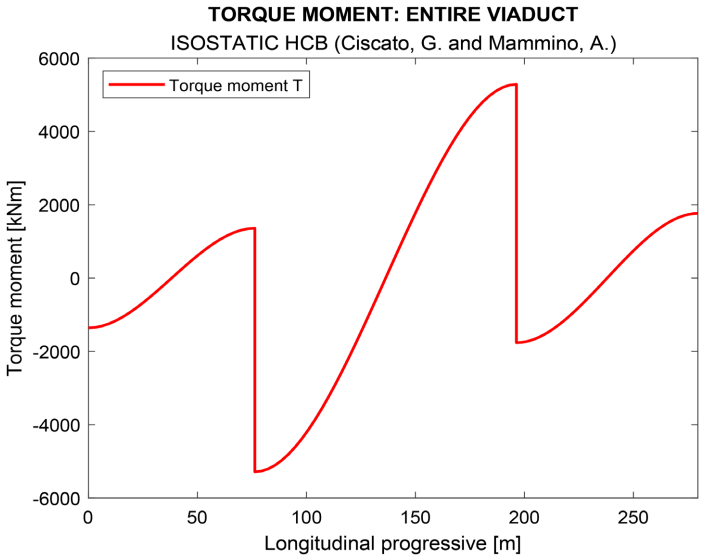

Figure 8. Entire viaduct. Torque diagrams of the Isostatic HCB, adopted in the original design, under the action of permanent loads.

3.1.2. Continuous HCB for the Bending Moment

In the original design, the bending moment was calculated by considering the bridge deck as a curved continuous beam on four supports (see **Figure 9**): this design choice turns out to be inconsistent with the computation of the torque moment diagram, but more adherent to reality with regard to the distribution of the bending moment. Based on the Principle of Virtual Works [20] [22] [23] [24] [25] [26] and starting from the straight continuous beam on $n + 2$ supports, the main isostatic structure must be identified by eliminating n constraints of the real structure [27] [28] [29] [30]: the bending rotation of the internal sup-

ports can be released and, consequently, the n hyperstatic unknowns are the moments of continuity at the internal supports.

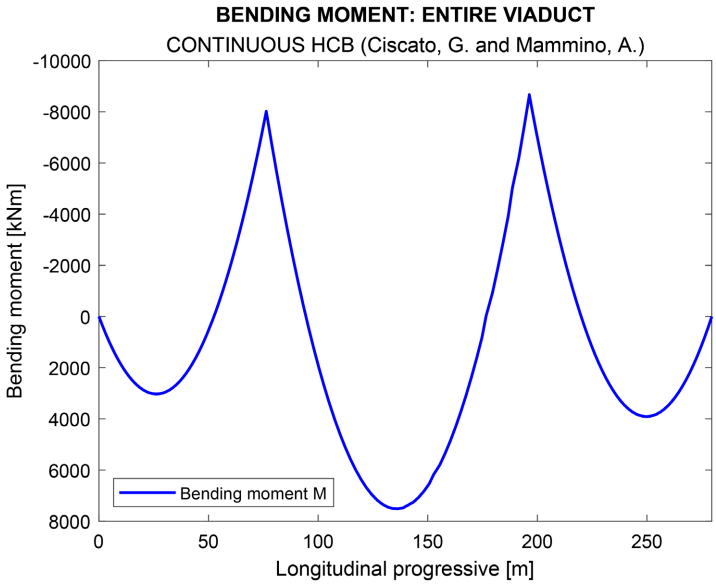

Figure 9. Entire viaduct. Bending moment diagram of the Continuous HCB, adopted in the original design, under the action of permanent loads.

In **Figure 10** N is the number of spans; $n=N-1$ represents the number of flexural hyperstatic unknowns; L_i is the span length and q is the uniformly distributed load applied to the single span. In the case of structural system constrained with rigid supports, the resolving system is made by n-linear algebraic equations of congruence t [20] which allow to derive the response of the structure in terms of internal stress diagrams.

$$\begin{bmatrix} \int_S \frac{M_{(1)}^2}{EI}\mathrm{ds} & \int_S \frac{M_{(1)}M_{(2)}}{EI}\mathrm{ds} & & 0 \\ \int_S \frac{M_{(2)}M_{(1)}}{EI}\mathrm{ds} & \int_S \frac{M_{(2)}^2}{EI}\mathrm{ds} & \ddots & \\ & \ddots & \ddots & \int_S \frac{M_{(n-1)}M_{(n)}}{EI}\mathrm{ds} \\ 0 & & \int_S \frac{M_{(n)}M_{(n-1)}}{EI}\mathrm{ds} & \int_S \frac{M_{(n)}^2}{EI}\mathrm{ds} \end{bmatrix} \begin{bmatrix} X_{1,1} & \cdots & X_{1,n} \\ X_{2,1} & \cdots & X_{2,n} \\ \vdots & \ddots & \vdots \\ X_{n,1} & \cdots & X_{n,n} \end{bmatrix} = \begin{bmatrix} P_{1,1} & \cdots & P_{1,n} \\ P_{2,1} & \cdots & P_{2,n} \\ \vdots & \ddots & \vdots \\ P_{n,1} & \cdots & P_{n,n} \end{bmatrix} \quad (3)$$

$$[E][X]=[P]\rightarrow[X]=[E]^{-1}[P]$$

where: $[E]$ is the flexibility matrix made of influence coefficients of dimension $n \cdot n$ (in the case of continuous rectilinear HCB the matrix $[E]$ is tri-diagonal and symmetrical); $[X]$ is matrix of the hyperstatic unknowns, of dimension $n \cdot n$ and $[P]$ is the matrix of the load conditions, of dimension $n \cdot n$:

$$P_{i,j}=\int_s M_{(i)} \cdot M_{(0)}\mathrm{ds}=\frac{1}{24}\cdot\left(q_{i,j}\cdot\frac{L_i^3}{I_i}+q_{i+1,j}\cdot\frac{L_{i+1}^3}{I_{i+1}}\right) \quad (4)$$

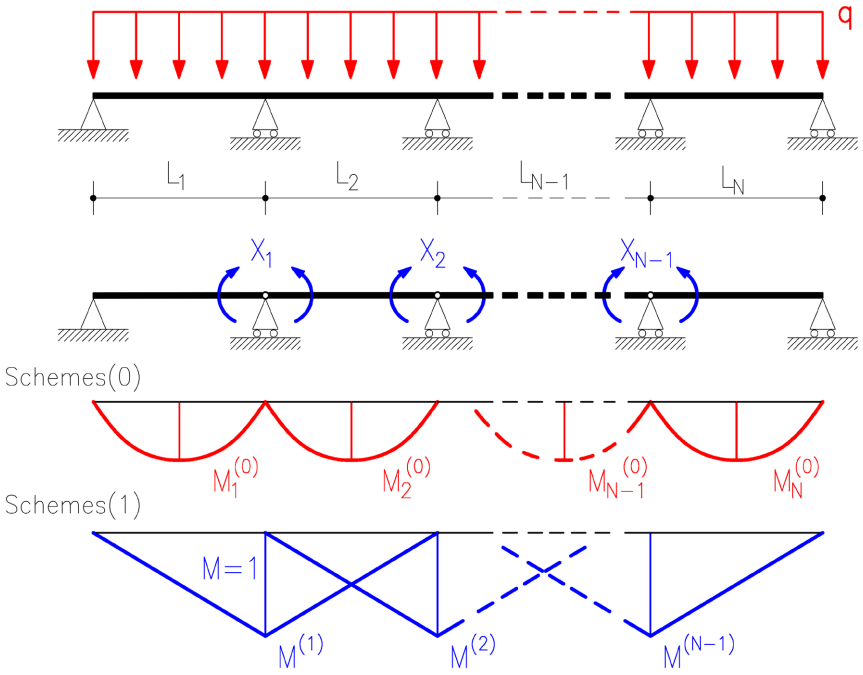

Figure 10. Continuous beam with n-spans, "scheme (0)" and $n = n - 1$ "scheme (1)".

By changing the terms of Equation (5) for the straight beam the terms of flexibility matrix are calculated from the following formulations:

- main diagonal ($i = 1, 2, \cdots, n$):

$$E_{i,i} = \frac{R_i}{4 \cdot E_i \cdot I_i} \left\{ \frac{\phi_{0,i}}{\left[\cos\left(\phi_{0,i}\right) \cdot \operatorname{sen}\left(\phi_{0,i}\right)\right]^2} - \frac{\cos^2\left(\phi_{0,i}\right) - \operatorname{sen}^2\left(\phi_{0,i}\right)}{\cos\left(\phi_{0,i}\right) \cdot \operatorname{sen}\left(\phi_{0,i}\right)} \right\} + \frac{R_{i+1}}{4 \cdot E_{i+1} \cdot I_{i+1}} \left\{ \frac{\phi_{0,i+1}}{\left[\cos\left(\phi_{0,i+1}\right) \cdot \operatorname{sen}\left(\phi_{0,i+1}\right)\right]^2} - \frac{\cos^2\left(\phi_{0,i+1}\right) - \operatorname{sen}^2\left(\phi_{0,i+1}\right)}{\cos\left(\phi_{0,i+1}\right) \cdot \operatorname{sen}\left(\phi_{0,i+1}\right)} \right\} \tag{5}$$

- lower diagonal ($i = 2, 3, \cdots, n$):

$$E_{i,i-1} = \frac{R_i}{4 \cdot E_i \cdot I_i} \left\{ \frac{1}{\cos\left(\phi_{0,i+1}\right) \cdot \operatorname{sen}\left(\phi_{0,i+1}\right)} - \frac{\phi_{0,i+1}}{\operatorname{sen}^2\left(\phi_{0,i+1}\right)} + \frac{\phi_{0,i+1}}{\cos^2\left(\phi_{0,i+1}\right)} \right\} \tag{6}$$

- upper diagonal ($i = 1, 2, \cdots, n-1$):

$$E_{i,i+1} = \frac{R_{i+1}}{4 \cdot E_{i+1} \cdot I_{i+1}} \left\{ \frac{1}{\cos\left(\phi_{0,i+1}\right) \cdot \operatorname{sen}\left(\phi_{0,i+1}\right)} - \frac{\phi_{0,i+1}}{\operatorname{sen}^2\left(\phi_{0,i+1}\right)} + \frac{\phi_{0,i+1}}{\cos^2\left(\phi_{0,i+1}\right)} \right\} \tag{7}$$

By adding the contributions of the hyperstatic unknowns and of the applied loads, in Equations (8) and (9), the overall one bending moment is $M_i^{tot} = M_i^X + M_i^K$:

$$M_i^X\left(\phi_i\right) = \frac{X_i + X_{i+1}}{2 \cdot \cos\left(\phi_{0,i}\right)} \cdot \cos\left(\phi_{0,i}\right) + \frac{X_{i+1} - X_i}{2 \cdot \operatorname{sen}\left(\phi_{0,i}\right)} \cdot \operatorname{sen}\left(\phi_{0,i}\right) \tag{8}$$

$$M_i^K\left(\phi_i\right) = k_{i,j} \left(\frac{\cos\left(\phi_i\right)}{\cos\left(\phi_{0,i}\right)} - 1 \right) \tag{9}$$

Following the discussion in refs. [20] and [21], on the other hand the shear ad torque diagrams follow that of the isostatic HCB as reported in Equations ((1), (2)).

3.2. Improved Analytical Modelling for the Torque Moment

The methodology used in the original design appears to be in favour of safety as it maximizes the effects of torsion at the stacks but assumes that the structure is isostatic in bending not considering that the real bending behaviour is that of a continuous beam: this difference is also observed by realizing the overall model of the viaduct.

For this reason, the torsion is recalculated considering each individual span extrapolated from the global structure and assuming that the twisting rotation is prevented on the supports and the bending rotation is free on the pile ends and prevented on the intermediate batteries, as shown in **Table 3**. This determines the following static diagrams: Hinged-Clamped for the C1 side span (P9 - P10), Clamped-Clamped for the C2 central span (P10 - P11) and Clamped-Hinged for the C3 span (P11 - P12).

The torsional stiffness factor of a single-linked [13] [31] hollow thin section is calculated according to the geometric characteristics reported in **Figure 11**.

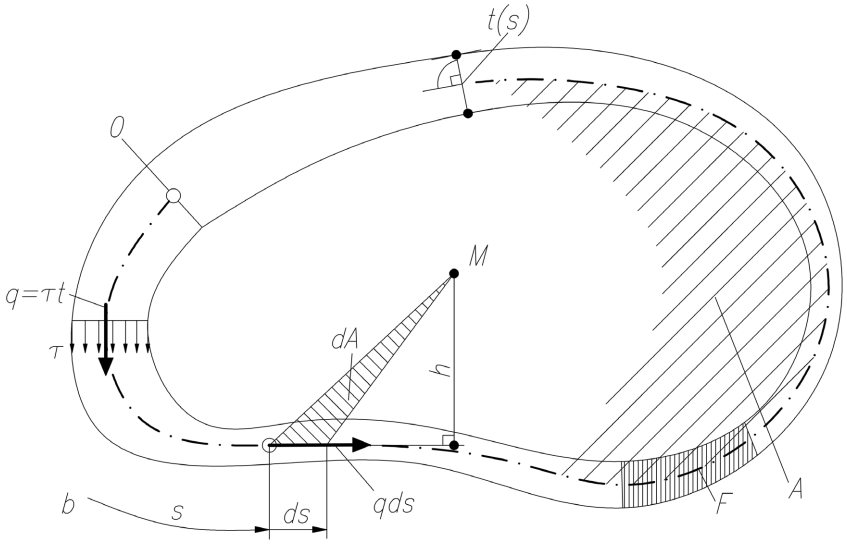

Figure 11. Geometric parameters for the calculation of the torsional stiffness factor for hollow thin sections [31].

3.2.1. Central Span

The span that best lends itself to the validation of the FEM results is the central span of 120 m, between piers P10 and P11, as the piers provide a bending constraint. The maximum dimensions for the box-girder section taken as reference are deducible from **Table 4** and **Figure 12**. From the theoretical treatment reported in ref. [32], the bending moment M_B and the torque moment T_B in correspondence with the piers axis are obtained (see **Table 5**) using Castigliano's

Theorem [22].

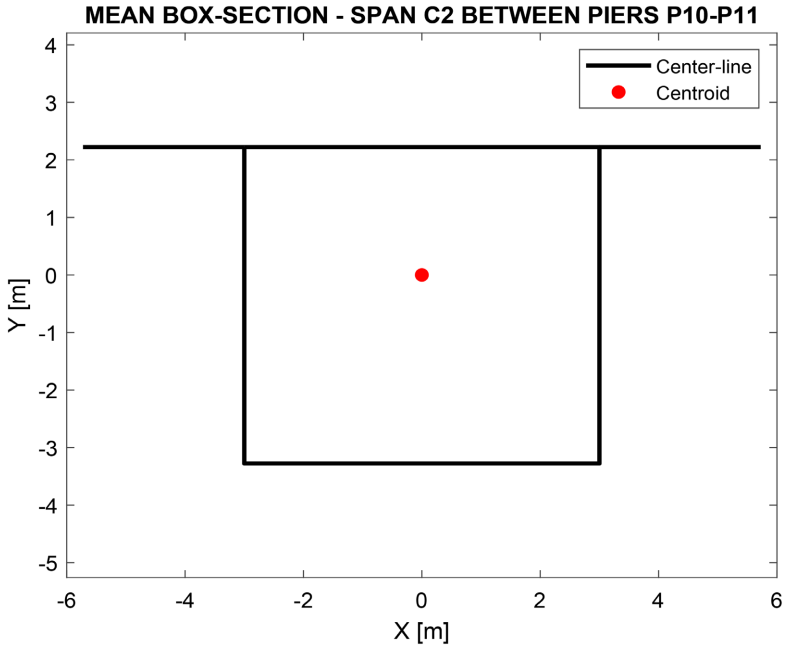

Figure 12. Center-line of the cross section of the span between P10 - P11 for the Clamped-Clamped HCB.

Using the values in **Table 5**, it is then possible to define the bending moment and torque diagrams using Equations (10) to (13) as the angle θ subtended by the generic point of the deck axis varies.

$$M(\theta) = q \cdot R^2 \cdot \left[\operatorname{sen}(\theta) \cdot \left(c_t - \frac{\theta}{2} \right) + \cos(\theta) \cdot (c_m - 1) + 1 \right] \tag{10}$$

$$T(\theta) = q \cdot R^2 \cdot \left[\operatorname{sen}(\theta) \cdot (\theta - c_m) - \cos(\theta) \cdot \left(c_t - \frac{\theta}{2} \right) - \frac{\theta}{2} \right] \tag{11}$$

where: θ is the angle defined by a generic point on the axis of the beam, from the node *j*; m is the ratio between flexural and pure torsional rigidities of the main girder as defined in Equation (12):

$$m = \frac{E \cdot I}{G \cdot J} = \frac{2(1+\upsilon) \cdot I}{J} \tag{12}$$

E is the Young Modulus; I is the moment of inertia of the cross section; G is the shear modulus, J is the torsional stiffness factor, υ is the Poisson's ratio, and c_m and c_t are the flexural and torsional constants as defined in Equation (13).

$$\begin{aligned} c_m &= \frac{2(m+1) \cdot \operatorname{sen}(\phi) - m \cdot \phi \cdot [1 - \cos(\phi)]}{\phi \cdot (m+1) - \operatorname{sen}(\phi) \cdot (m+1)} - 1 \\ c_t &= \frac{2(m+1) \cdot [1 - \cos(\phi)] - m \cdot \phi \cdot \operatorname{sen}(\phi)}{\phi \cdot (m+1) - \operatorname{sen}(\phi) \cdot (m+1)} - \frac{\phi}{2} \end{aligned} \tag{13}$$

Table 5. 120 m span between P10 and P11 - Solution of the hyperstatic HCB stuck at the ends subjected to permanent loads.

ANALYTICAL CALCULATION (Wong, Y.C.)			
Coefficient m	m	2.09	[–]
Radius of curvature	R	1200.00	[m]
Span length	$L_{P10-P11}$	120.00	[m]
Angle subtended by the span	ϕ	0.10000	[rad]
Distance between the center of curvature and the centroid of the arc	OG	1199.50	[m]
Rise of the arch	f	1.50	[m]
Uniformly distributed load	w	88.00	[kN/m]
Constraint reaction	F_b	5280.00	[kN]
Torsion coefficient	c_t	2.14E−08	[–]
Bending coefficient	c_m	8.34E−04	[–]
Bending moment at supported extreme B	M_B	105,671.79	[kNm]
Torque moment at supported extreme B	T_B	2.71	[kNm]

The diagrams of the bending and torque moments of the hyperstatic HCB, reported in Figure 13, are strongly different from those of the isostatic case: in the former case torsion assumes low values at the clamped-ends and the maximum values at about a quarter and three quarter of the span, whereas in the latter case the maximum torsion is located at the ends and assumes null values in the center of the span.

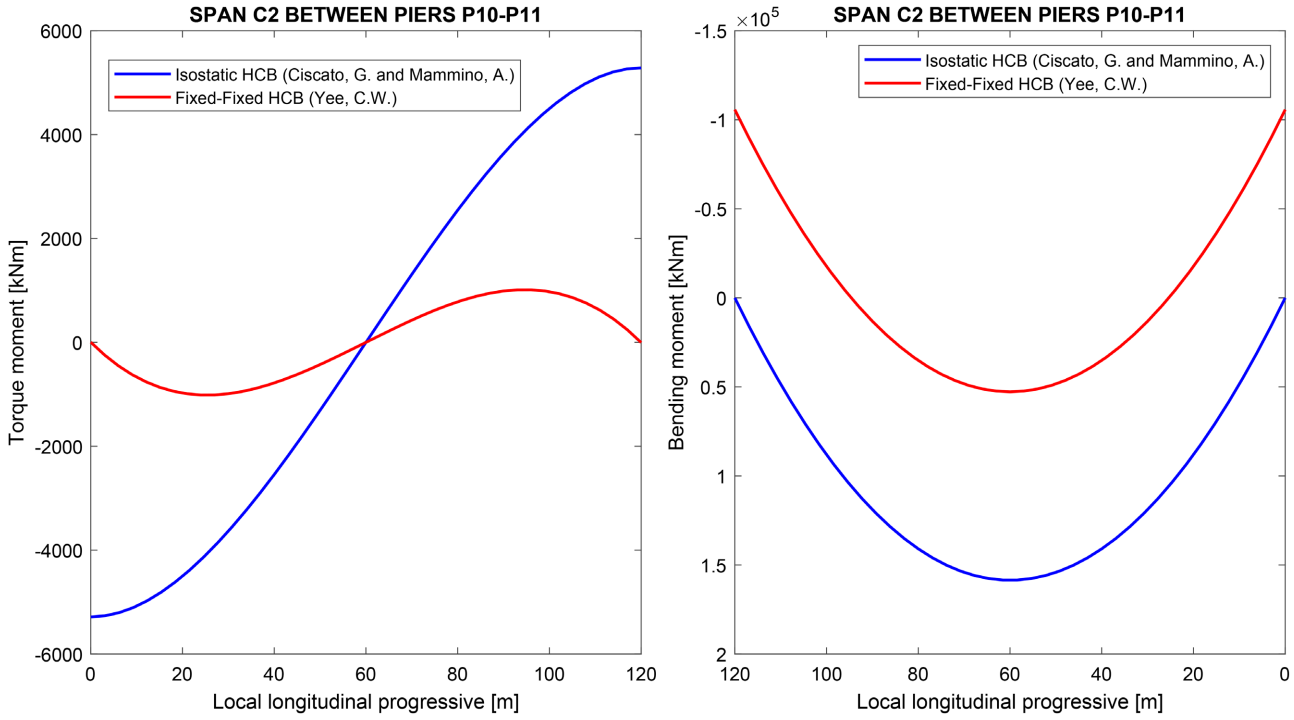

Figure 13. Torque (left) and bending moment (right) diagram for the isostatic and Clamped-Clamped HCB, under the action of permanent loads for the span P10 - P11.

3.2.2. Side Spans

The comparison of the results that can be obtained from the two analytical calculation methods described in the previous section for the determination of the torsional structural response, in particular of the torque stress characteristic, is now proposed for the side spans.

The torsion problem of the 76.33 m long lateral span of the South carriageway is solved extrapolating it from the structural context [21] [23] and solving the static scheme of the HCB clamped in pier P10 and hinged in pier P9 (refer to Figure 3). The maximum dimensions for the box-girder section taken into account are summarized are deducible from Figure 14 and Figure 15.

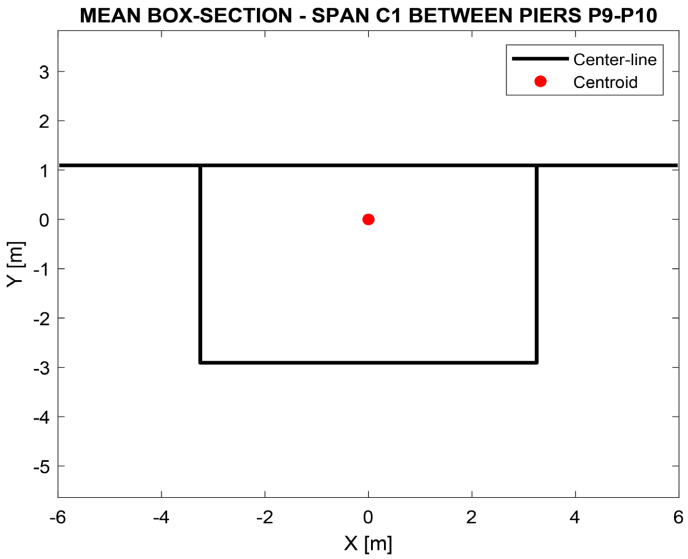

Figure 14. Center-line of the cross section of the span between P9 - P10 for the Hinged-Clamped HCB.

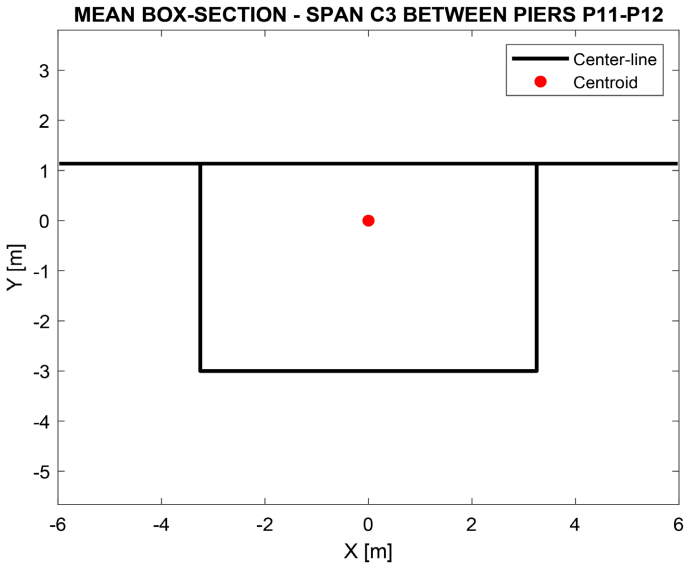

Figure 15. Center-line of the cross section of the span between P11 - P12 for the Clamped-Hinged HCB.

The vertical reaction R_A and the torque moment T_A at the supported end have been computed following the procedure proposed in ref. [23]. Their values are reported in **Table 6**. The bending and torque moments due to the distributed load uniformly applied to the circular cantilever beam are given in Equation (14):

$$\begin{aligned} M^q(\omega) &= \int_0^{\omega} -q \cdot R^2 \cdot \operatorname{sen}(\omega - \varepsilon) \mathrm{d}\varepsilon = -q \cdot R^2 \left[1 - \cos(\omega)\right] \\ T^q(\omega) &= \int_0^{\omega} q \cdot R^2 \cdot \left[1 - \cos(\omega - \varepsilon)\right] \mathrm{d}\varepsilon = q \cdot R^2 \left[\omega - \operatorname{sen}(\omega)\right] \end{aligned} \tag{14}$$

The Hinged-Clamped static scheme can be analysed from the known problem of the isostatic cantilever curved beam, by assuming the boundary reactions at the free-end ($R_{v,A}$, M_A and T_A shown in **Figure 16**) as unknowns and imposing the corresponding boundary constraints through the displacement and rotational congruence equations at the extreme A, given in Equation (15).

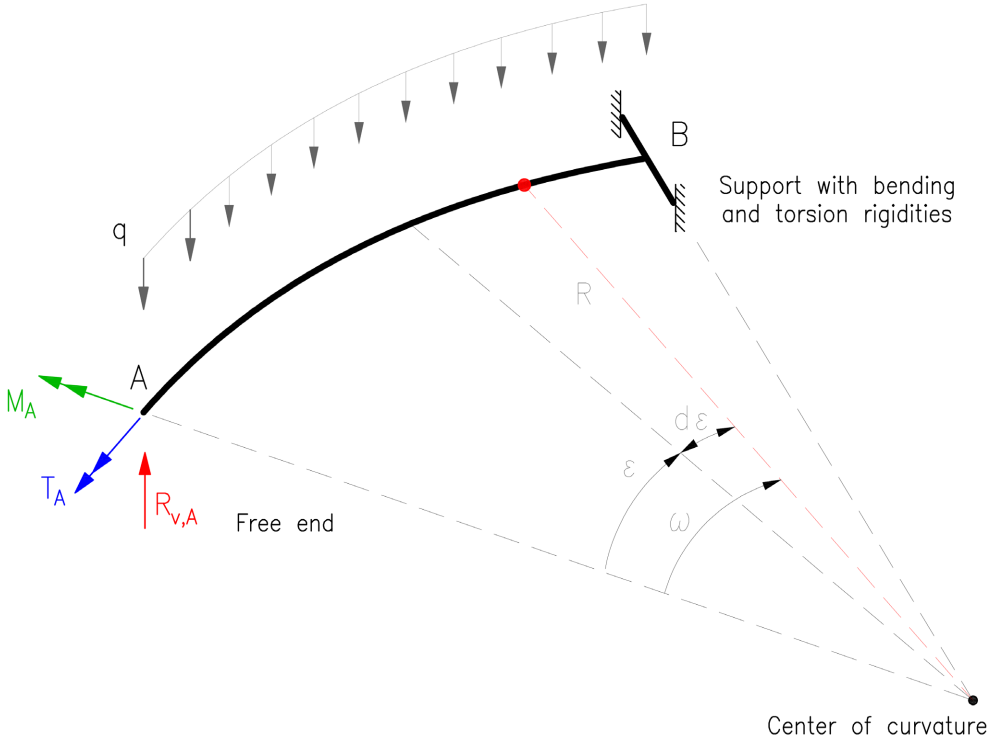

Figure 16. Cantilever circular beam subjected to a uniformly distributed load and the $R_{v,A}$, T_A and M_A forces at the free end.

The problem is statically determined, as it consists of a system of three equations in three unknowns.

$$\begin{cases} \zeta_A^{Rv,A} + \zeta_A^q = 0 \rightarrow R_{v,A} & \text{(15-a)} \\ \vartheta_A^{Rv,A} + \vartheta_A^q + \vartheta_A^{T,A} + \vartheta_A^{M,A} = 0 \rightarrow T_A & \text{(15-b)} \\ \varphi_A^{Rv,A} + \varphi_A^q + \varphi_A^{T,A} + \varphi_A^{M,A} \neq 0 \rightarrow M_A = 0 & \text{(15-c)} \end{cases}$$

Equation (15-a) shows that imposing the vertical displacement equal to zero

[24] by superposing the effect of the vertical constraint reaction $\zeta_A^{Rv,A}$ and of the uniformly distributed load ζ_A^q, see Equations (16) and (17), it is possible to derive the vertical constraint reaction in A.

$$\zeta_A^{Rv,A} = \frac{1}{EI}\int_0^{\phi} R_{v,A}\cdot R^3\cdot \mathrm{sen}^2(\omega)\,\mathrm{d}\omega + \frac{1}{GJ}\int_0^{\phi} R_{v,A}\cdot R^3\cdot\left[1-\cos(\omega)\right]^2\,\mathrm{d}\omega \quad (16)$$

$$\begin{aligned}\zeta_A^q = {} & \frac{1}{EI}\int_0^{\phi} q\cdot R^4\cdot\left[1-\cos(\omega)\right]\cdot\mathrm{sen}(\omega)\,\mathrm{d}\omega \\ & + \frac{1}{GJ}\int_0^{\phi} q\cdot R^4\cdot\left[\omega-\mathrm{sen}(\omega)\right]\cdot\left[1-\cos(\omega)\right]\mathrm{d}\omega\end{aligned} \quad (17)$$

Similarly, Equation (15-b) shows that cancelling the torsional rotation at the node A due to the load ϑ_A^q, the vertical reaction $\vartheta_A^{Rv,A}$, the torque $\vartheta_A^{T,A}$ and bending moment $\vartheta_A^{M,A}$ the torque offered by the additional support constraint T_A is obtained.

$$\vartheta_A^{Rv,A} = \frac{1}{EI}\int_0^{\phi} R_{v,A}\cdot R^2\cdot\mathrm{sen}^2(\omega)\,\mathrm{d}\omega - \frac{1}{GJ}\int_0^{\phi} R_{v,A}\cdot R^2\cdot\left[1-\cos(\omega)\right]\cdot\cos(\omega)\,\mathrm{d}\omega \quad (18)$$

$$\begin{aligned}\vartheta_A^q = {} & -\frac{1}{EI}\int_0^{\phi} q\cdot R^3\cdot\left[1-\cos(\omega)\right]\cdot\mathrm{sen}(\omega)\,\mathrm{d}\omega \\ & + \frac{1}{GJ}\int_0^{\phi} q\cdot R^3\cdot\left[\omega-\mathrm{sen}(\omega)\right]\cdot\cos(\omega)\,\mathrm{d}\omega\end{aligned} \quad (19)$$

$$\vartheta_A^{T,A} = \frac{1}{EI}\int_0^{\phi} T_A\cdot R^2\cdot\mathrm{sen}^2(\omega)\,\mathrm{d}\omega - \frac{1}{GJ}\int_0^{\phi} T_A\cdot R^2\cdot\left[1-\cos(\omega)\right]\cdot\cos(\omega)\,\mathrm{d}\omega \quad (20)$$

$$\vartheta_A^{M,A} = \frac{1}{EI}\int_0^{\phi} M_A\cdot R\cdot\mathrm{sen}(\omega)\cdot\cos(\omega)\,\mathrm{d}\omega - \frac{1}{GJ}\int_0^{\phi} M_A\cdot R\cdot\mathrm{sen}(\omega)\cdot\cos(\omega)\,\mathrm{d}\omega \quad (21)$$

The bending moment M_A can be neglected as there is a flexural hinge in the extremity A that provide free rotation $\varphi_A^{M,A}$. Finally, bending and torque moments in a generic point along the axis of the beam are provided by Equations (22) and (23) as a function of the boundary reactions applied to the support A of the beam.

$$\begin{aligned}M(\omega) &= M^{Rv,A} + M^q + M^{T,A} + M^{M,A} \\ &= R_{v,A}\cdot R\cdot\mathrm{sen}(\omega) - q\cdot R^2\cdot\left[1-\cos(\omega)\right]\cdot\mathrm{sen}(\omega) \\ &\quad + M_A\cdot\cos(\omega) + T_A\cdot\mathrm{sen}(\omega)\end{aligned} \quad (22)$$

$$\begin{aligned}T(\omega) &= T^{Rv,A} + T^q + T^{T,A} + T^{M,A} \\ &= -R_{v,A}\cdot R\cdot\left[1-\cos(\omega)\right] + q\cdot R\cdot\left[\omega-\cos(\omega)\right] \\ &\quad - M_A\cdot\mathrm{sen}(\omega) + T_A\cdot\cos(\omega)\end{aligned} \quad (23)$$

By replacing the values of the reactions provided in **Table 6** in Equations (22) and (23) it is possible to derive the diagrams of the bending and torque moment along the deck axis. The comparison between the analytical calculation of the hyperstatic Hinged-Clamped HCB and the isostatic Hinged-Hinged case, is reported in **Figure 17**.

Table 6. 76.33 m long span C2 (P9 - P10)—Solution of the hyperstatic HCB Clamped-Hinged at the extremities and subjected to permanent loads.

BENDING AND TORQUE MOMENT AT THE EXTREMITY A (from ref. [23] Belluzzi, O.)			
Stiffness ratio	m	2	[−]
Radius of curvature	R	1200.00	[m]
Span length	$L_{P10-P11}$	120.00	[m]
Angle subtended by the span	ϕ	0.10	[rad]
Distance between center of curvature and the centroid of the arc	OG	1199.50	[m]
Rise of the arch	f	0.61	[m]
Uniformly distributed load	w	88.00	[kN/m]
Constraint reaction	F_A	2518.55	[kN]
Bending moment at supported joint B	M_A	0.00	[kNm]
Torque moment at supported joint B	T_A	−680.38	[kNm]

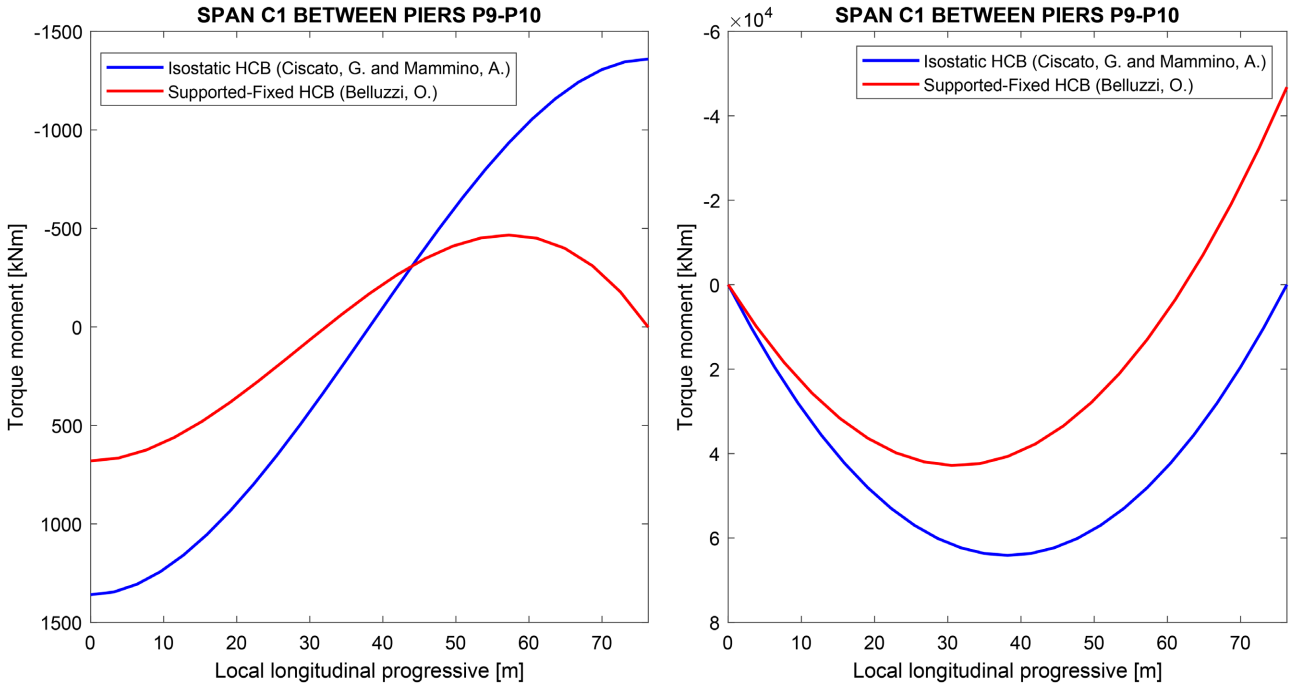

Figure 17. Torque (left) and Bending moment (right) diagrams of the side span, in the Isostatic and Hinged-Clamped configurations, under the action of permanent loads.

For the side spans, the redistribution of the torque and bending moments, compared to the isostatic case, is affected only by the presence of a clamped-end that leads to maximum torsion where the bending moment is null and vice-versa for the minimum values. At the annulment of the bending moment there is the maximum torsion at about three quarters of the span.

4. Numerical Models

Given the complexity of the real geometric configuration of the viaduct, the creation of a finite element model is a useful support to the design. The local (single span) and global (continuous girder) numerical models of the entire viaduct created with Midas GEN® and DIANA FEA® are described to understand the torsional response under uniformly distributed loads which represents a standard case that can also be treated analytically by comparing the results.

4.1. Central Span

The central span (C2) of the viaduct is analyzed through two distinct FEM models in Midas GEN®, whose boundary conditions can be summarized in **Table 3** and **Table 7**. The first FEM model "1-C2", as validation of the results obtained with the theoretical treatment [32] to which the geometric characteristics reported in **Table 5** have been assigned, is representative of the approximate geometric configuration with a radius of curvature equal to 1200 m and symmetrical planimetric configuration. The second FEM model "2-C2" has the same planimetric configuration as the model "1-C2" previously described, with the difference that the geometric characteristics (see **Table 4**) deriving from the as-built have been assigned to the beam elements. In the diagrams in **Figure 18** it can be seen that, neglecting the discontinuities due to the presence of the mesh nodes, the response of the FEM model is in agreement with the analytical one and the results are very sensitive to the real variation of the cross section. The torque moment is influenced by the stiffness of the structural element, because the constraint condition is hyperstatic, and by the position in the space [4] of the arc of the circle that approximates the clothoidal layout of the span considered.

Table 7. Main differences of the FEM models of spans C2 and C3 extrapolated from the structural context.

FEM MIDAS GEN	BOX-SECTION TYPE	PIER CONSTRAIN	
		Node-i	Node-j
1-C2	Equivalent	Clamped-end	Clamped-end
2-C2	Real		
1-C3	Equivalent	Clamped-end	Clamped-end with beam-end-release
2-C3	Real		
3-C3	Equivalent		External roller
4-C3	Real		

4.2. Side Span

Four FE models are created, as validation of the results of the side span C3 that can be obtained with the theoretical treatment [23], in which the mechanical and geometric characteristics of the viaduct longitudinal axis (assumed symmetrical

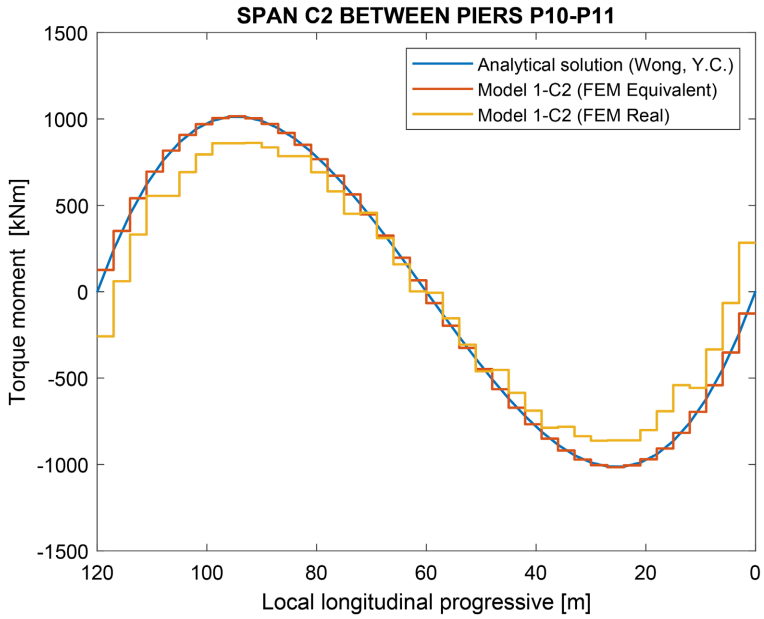

Figure 18. Span P10 - P11, Torque diagram, under the action of permanent loads.

with a counter-clockwise curve with a radius of curvature equal to 1200 m) are unchanged but the constraint conditions and the geometric characteristics of the cross sections are modified:

- model "1-C3" has cross-section equivalent to the real ones (see **Figure 17**) and with a clamped constraint at the right end but with the peculiarity of releasing the bending rotation at the node of the pile P12 (see **Table 7**);
- model "2-C3" is similar to the previous one by modifying the mesh sections by attributing the different sections as deducible from the as-built (see **Table 4**);
- model "3-C3" is equal to "1-C3" but the constraint condition is changed making it similar to the one that will be used in the model of the entire viaduct: an external hinge is assigned to the node in correspondence of the pier P12;
- model "4-C3" is equal to "2-C3" but in correspondence of the pier P12 an external hinge is assigned as in "4-C3".

The results of the solution of the equations relating to torque and bending are reported in **Figure 19** together with those deriving from the four FEMs of the third span. Given the hyperstatic constraint condition, the influence of torsional stiffness is relevant: which is evident in the constraint of changing pier P12 in Midas GEN®, in the models "2-C3" and "4-C3". This influence, on the other hand, is not highlighted in the models "1-C3" and "3-C3".

4.3. Global Models of the Viaduct

The case study is analyzed with two global models (see **Figure 20**), with Midas Gen® and with DIANA FEA®. The first model mentioned provides a linear variation of the elements' thicknesses, while the second model identifies an average

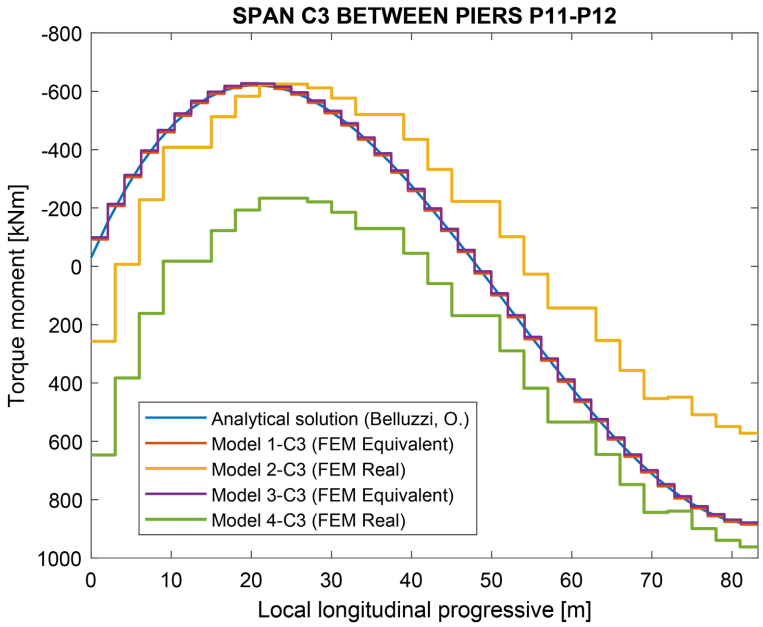

Figure 19. Span P11 - P12, Torque diagram, under the action of permanent loads.

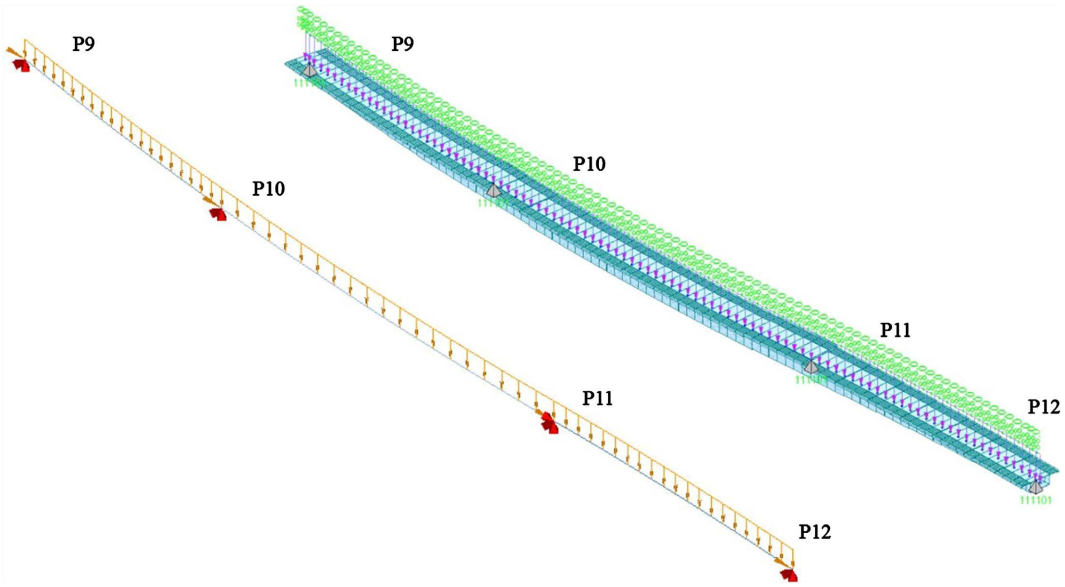

Figure 20. FEMs of entire viaduct in DIANA FEA® (left) and in Midas GEN® (right).

section for each span and the one-dimensional elements are of each span are curving without forcing a linear interpolation of the curvilinear spans of the viaduct.

5. Results and Discussion

The comparison between the results obtained from the FEM models in Midas GEN® and DIANA FEA® (see **Figures 21-23**) and from the analytical calculation are reported in this section.

As shown in **Figure 21**, the maximum torque moments occur along the cen-

tral span, close to the quarter points. On the other hand, torsional moments are relatively high at the pier locations and viaduct ends where there are the abutments whereas decrease toward the mid-spans.

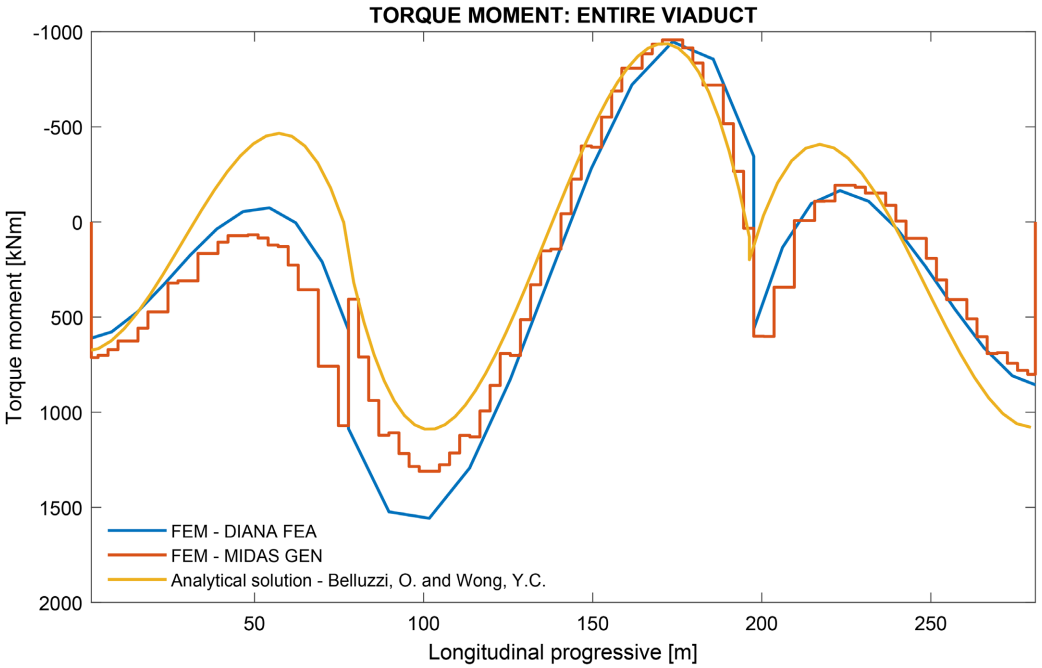

Figure 21. Comparison of the torque moment for permanent loads.

Bending moment (**Figure 22**) and shear diagrams (**Figure 23**) have the typical trend of straight continuous beam.

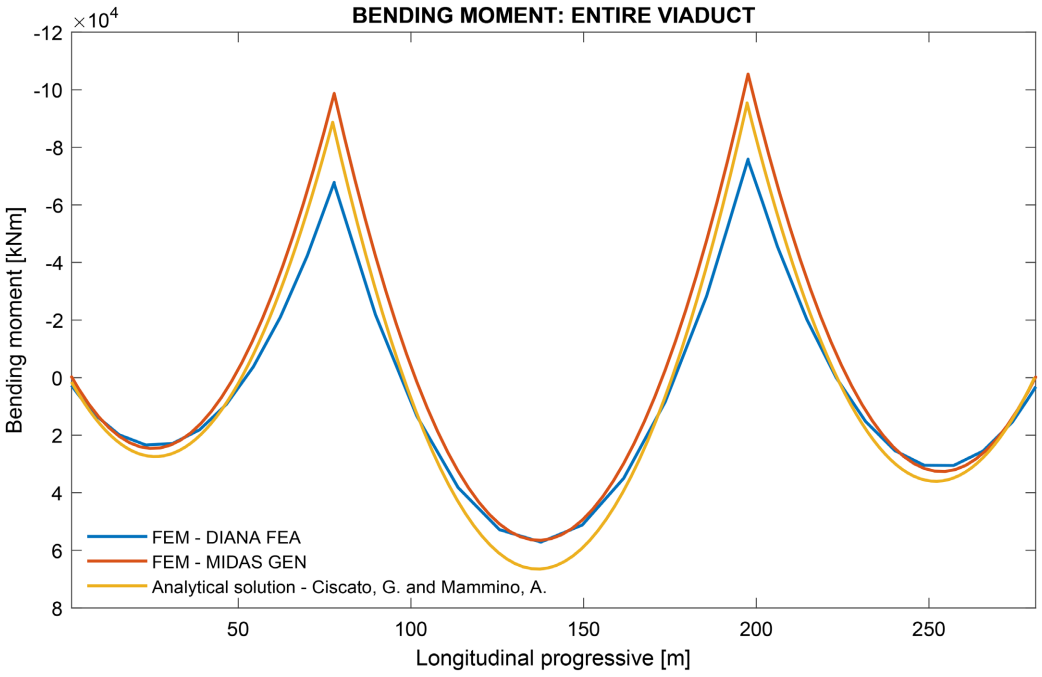

Figure 22. Comparison of the bending moment for permanent loads.

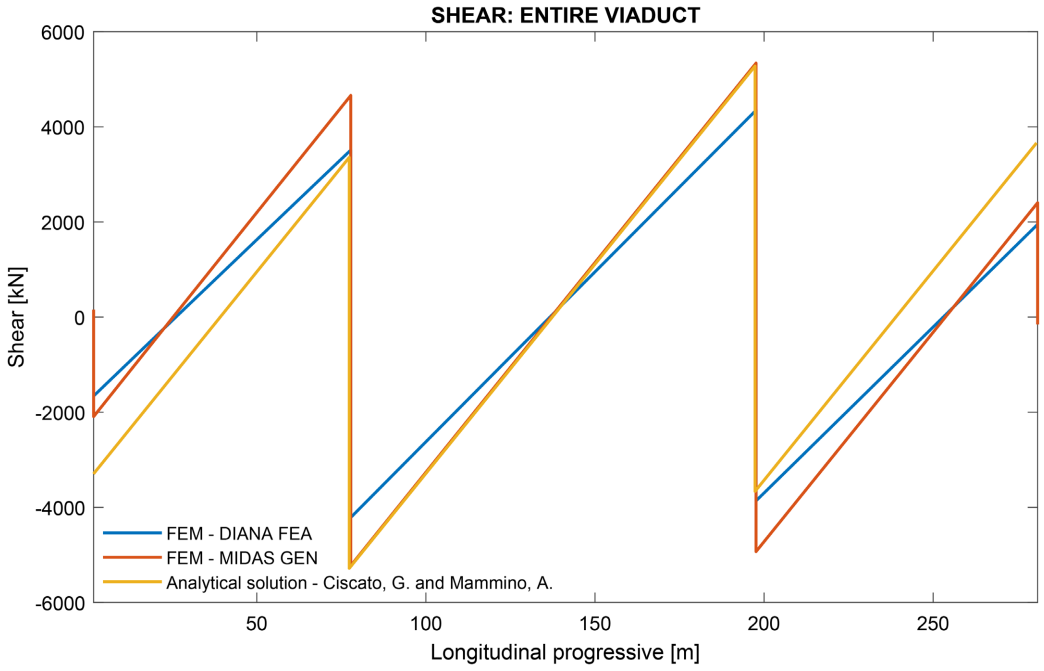

Figure 23. Comparison of the shear for permanent loads.

6. Conclusions

In this paper, the analytical solution to evaluate the torsional and bending actions for horizontally curved beams (HCB) has been faced. The case study presented was originally designed with the theory of the isostatic balcony, that simplified the calculations providing conservative results. Today, however, it is very common to derive the characteristics of the stresses from sophisticated and complex finite element (FE) models, but it is always necessary to check the results because of the strong hypotheses that are usually introduced in the modelling. With the proposed approach, the HCB theory is compared to the results of FE modelling in Midas Gen and Diana FEA. The following aspects are then highlighted:

- Curved girders are modeled using straight beam elements in Midas GEN®. The theoretical formulations of the software assume that the torsional moment within an element is constant, since modeling the HCB using curved elements is not possible. With more refined mesh there is better resemblance with the theoretical behavior even though this is still not close to reality.
- Approximation of the planimetric configuration: the FEMs are representative of the approximate configuration of the viaduct spans assuming a constant radius, and differ from the standard planimetric configurations assumed in the theoretical treatises given the geometric complexity of the viaduct.
- Different cross-sections in the global models: the two FEMs considered different modeling of the cross-sections. In Midas Gen the viaduct was discretized to capture the linear variation of the height of the caisson and the variation of the thicknesses of the lower and upper sheets of the caisson, while in

DIANA FEA® only three middle sections of each span were used. Some differences emerge due to the constant cross-sectional area approximation for analytical solutions.

- Simulation of the constraints of the intermediate piers P10 and P11: for the analytical solution of the torsion of the HCB it has been assumed that in correspondence of P10 and P11 the bending moment derives from the ideal static scheme of Hinged-Clamped beam (considering the span as extrapolated from structural context). Instead in FEMs the deck is a continuous beam on four supports and the two internal piers do not interrupt the structural continuity.

The simplified analytical methods proposed in this research represent a valid tool that the designer can use as quick analytical validation of the results obtained from sophisticated linear static analyses to appreciate the real behavior of box-girder bridges with a clothoidal planimetric layout.

Conflicts of Interest

The authors declare no conflicts of interest regarding the publication of this paper.

References

[1] Ziemian, R.D. (2010) Guide to Stability Design Criteria for Metal Structures, Horizontally Curved Steel Girders. 6th Edition, John Wiley & Sons, Inc., Hoboken, 412-455.

[2] Hambly, E.C. (1991) Bridge Deck Behaviour. 2nd Edition, CRC Press, Boca Raton, London. https://doi.org/10.1201/9781482267167

[3] Li, W.Y., Tham, L.G. and Cheung, Y.K. (1988) Curved Box-Girder Bridges. Journal of Structural Engineering, **114**, 1324-1338. https://doi.org/10.1061/(ASCE)0733-9445(1988)114:6(1324)

[4] Villaggio, P. (1997) Mathematical Models for Elastic Structures. Cambridge University Press, Cambridge.

[5] Hirt, M. and Lebet, J.P. (2013) Steel Bridges: Conceptual and Structural Design of Steel and Steel-Concrete Composite Bridges. 1st Edition, CRC Press, Boca Raton, London.

[6] Heins, C.P. and Oleinik, J.C. (1976) Curved Box Beam Bridge Analysis. *Computers & Structures*, **6**, 65-73. https://doi.org/10.1016/0045-7949(76)90054-7

[7] Sennah, K.M. and Kennedy, J.B. (2001) State of the Art in Design of Curved Box-Girder Bridges. *Journal of Bridge Engineering*, **6**, 159-167. https://doi.org/10.1061/(ASCE)1084-0702(2001)6:3(159)

[8] Fu, C.C. and Wang, S. (2014) Computational Analysis and Design of Bridge Structures. CRC Press, Boca Raton, London.

[9] Helwig, T.A., Yura, J., Herman, R., Williamson, E. and Li, D. (2007) Design Guidelines for Steel Trapezoidal Box Girder Systems. Center for Transportation Research, The University of Texas at Austin, Austin.

[10] European Committee for Standardization (2005) EN 1991-2 Eurocode 1: Actions on Structures Part 2: Traffic Loads on Bridges.

[11] Chen, W.-F. and Duan, L. (2014) Bridge Engineering Handbook. 2nd edition, CRC Press, Boca Raton, London.

[12] Richard Liew, J.Y., Thevendran, V., Shanmugam, N.E. and Tan, L.O. (1995) Behaviour and Design of Horizontally Curved Steel Beams. *Journal of Constructional Steel Research*, **32**, 37-67. https://doi.org/10.1016/0143-974X(94)00011-6

[13] Timoshenko, S.P. and Goodier J.N. (1985) Theory of elasticity. McGraw Hill, New York.

[14] Mairone, M., Asso, R., Masera, D., Invernizzi, S., Montagnoli, F. and Carpinteri, A. (2022) The Phenomenon of Fatigue in Existing Orthotropic Steel Deck (OSD) Bridges. *Infrastructures*, **7** (Manuscript Submitted for Publication).

[15] European Committee for Standardization (2005) EN 1993-1-1 Eurocode 3: Design of Steel Structures Part 1-1 General Rules and Rules for Buildings.

[16] Mairone, M., Asso, R., Masera, D. and Palumbo, P. (2022) Fatigue Damage in Existing Box-Girder Orthotropic Steel Bridges Deck (OSD). *Proceedings of the XXVIII Giornate Italiane della Costruzione in Acciaio*, Francavilla al mare (CH), 29 September-1 October 2022, (Submitted for publication).

[17] Asso, R., Cucuzza, R., Rosso, M.M., Masera, D. and Marano, G.C. (2021) Bridges Monitoring: An Application of AI with Gaussian Processes. *Proceedings of the* 14*th International Conference on Evolutionary and Deterministic Methods for Design, Optimization and Control*, Athens, 28-30 June 2021, 245-261. https://doi.org/10.7712/140121.7964.18426

[18] European Committee for Standardization (2007) EN 1993-2 Eurocode 3: Design of Steel Structures: Steel Bridges. Brussels, European Committee for Standardization Part 2: Steel Bridges.

[19] Mairone, M., Asso, R., Masera, D., and Palumbo, P. (2022) Torsional Behaviour of an Existing Viaduct with Horizontally Curved Steel Box-Girder Deck. Proceedings of the *XXVIII Giornate Italiane della Costruzione in Acciaio,* Francavilla al mare (CH), 29 September-1 October 2022, (Submitted for publication).

[20] Ciscato, G. and Mammino, A. (1987) Un solaio chiamato predalle: Disegni, particolari, calcoli. Alinea, Firenze.

[21] Nakai, H. and Yoo, C.H. (1988) Analysis and Design of Curved Steel Bridges. McGraw-Hill, New York.

[22] Castigliano, A. (1873) Intorno ai Sistemi Elastici; Dissertazione presentata da Castigliano Alberto alla Commissione Esaminatrice della R. Scuola d'applicazione degli Ingegneri in Torino. Bona, Torino.

[23] Odone, B. (1966) Scienza delle costruzioni 2. Zanichelli, Bologna.

[24] Mairone, M. (2021) Study of an Existing Viaduct with Box-Girder Orthotropic Steel Deck. MSc Thesis, Politecnico di Torino, Torino.

[25] Colonnetti, G. (1927) I Fondamenti Della Statica. Unione Tipografico-Editrice Torinese (UTET), Torino.

[26] Antona, E. and Carrera, E. (1993) Nota sul principio dei lavori virtuali, Scritti e testimonianze in ricordo di Attilio Lausetti Politecnico di Torino, Dipartimento di Ingegneria Aeronautica e Spaziale.

[27] Bedenik, B.S. and Besant, C.B. (1999) Analysis of Engineering Structures. Woodhead Publishing Series in Civil and Structural Engineering, Woodhead Publishing, Sawston. https://doi.org/10.7712/140121.7964.18426

[28] Carpinteri, A. (2017) Advanced Structural Mechanics. 1st Edition, CRC Press, Boca

Raton, London. https://doi.org/10.1201/9781315375298

[29] Carpinteri, A. (2017) Structural Mechanics—A Unified Approach. 1st Edition, CRC Press, Boca Raton, London.

[30] Carpinteri, A. (2013) Structural Mechanics Fundamentals. CRC Press, Boca Raton, London. https://doi.org/10.1201/b15741

[31] Kollbrunner, C.F. and Basler, K. (1966) Torsion. Springer, Berlin. https://doi.org/10.1007/978-3-662-29648-6

[32] Wong, Y.C. (1969) Horizontally Curved Beam Analysis and Design. MSc Thesis, Oregon State University, Oregon.